Sedative choice alters *Klebsiella pneumoniae* lung pathogenesis and dissemination

David Mains[1†*], Ella R. Rotman[2§*], Deanna K. Aman[3*], Denise A. Ludvik[4], Anirudh Desikan[4||], Acadia A. Kocher[2#], Mark J. Mandel[2,4], Nancy E. Freitag[1,3]

[1]Department of Microbiology and Immunology, University of Illinois at Chicago, Chicago, IL 60612

[2]Department of Microbiology-Immunology, Northwestern University Feinberg School of Medicine, Chicago, IL 60611

[3]Department of Pharmaceutical Sciences, University of Illinois, Chicago, IL 60611

[4]Department of Medical Microbiology and Immunology, University of Wisconsin-Madison, Madison, WI 53706

* Equal Contribution

[†] Current Address: Corporate Research and Development, Solventum, Maplewood, MN 55144.

[§] Current Address: Department of Microbiology, University of Chicago, Chicago, IL 60637

[||] Current Address: Statistics and Machine Learning Department, Boston University, Boston, MA 02215

[#] Current Address: Division of Molecular Genetics and Oncode Institute, Netherlands Cancer Institute, Amsterdam, The Netherlands

Short title: *K. pneumoniae* virulence influenced by anesthesia exposure

Keywords: Klebsiella pneumoniae, transposon insertion sequencing (INSeq/Tn-seq), pneumonia, propofol, ketamine, virulence

Correspondence to:

Mark J. Mandel
University of Wisconsin-Madison
Department of Medical Microbiology and Immunology
1550 Linden Drive, MSB 5155
Madison, WI 53706
Phone: (608) 261-1170
Email: mmandel@wisc.edu

Nancy E. Freitag
Department of Pharmaceutical Sciences
University of Illinois
Chicago, IL 60611
Phone: (312) 355-4903
Email: nfreitag@uic.edu

ABSTRACT (208 Words)

Klebsiella pneumoniae make up 85% of Carbapenem-resistant Enterobacteriaceae (CRE), bacteria that have become an urgent threat to public health. *K. pneumoniae* is largely transmitted in healthcare settings, where inpatients and outpatients are often anesthetized with the ubiquitously-used anesthetic induction agent propofol. Recent evidence indicates that propofol exposure can dramatically increase host susceptibility to microbial infections. Given that intubated patients are often given propofol and are at risk for *K. pneumoniae* lung infections, we investigated the outcome of *K. pneumoniae* infections in mice briefly sedated with either propofol or ketamine/xylazine as control. Propofol-sedated mice experienced more rapid dissemination from the lungs to secondary sites of infection and developed more severe lung pathology. Based on these observations, we investigated bacterial factors involved in infection and dissemination in mice with and without propofol sedation using a high throughput insertion sequencing (INSeq) approach. We identified numerous novel potential virulence factors together with previously identified gene products, confirming the validity of our screen. We further identified insertion mutants with differing degrees of attenuation dependent upon sedation method. These results highlight the importance of sedative choice when studying hospital-acquired microbial infections and suggest that sedation can influence the arsenal of bacterial virulence factors required to promote *K. pneumoniae* infection and dissemination in animal models.

IMPORTANCE

Host sedation by either propofol or ketamine exposure varied the genetic requirements for *K. pneumoniae* during an intranasal mouse model of lung infection. This unprecedented result offers a deeper understanding of virulence factor function dependence on host immunity following sedation. Given the dominating use of propofol in health care settings and during

intubation in the ICU, this work also provides important perspective as to how the choice of an anesthetic agent can impact the outcome of healthcare-associated infections.

INTRODUCTION

Healthcare-associated infections (HAIs) are a significant risk for patients undergoing invasive procedures. The risk of HAIs increases with length of stay, surgery, and more recently acknowledged, anesthesia (1). Patients requiring mechanical ventilation are frequently administered sedatives (2) and are at increased risk for a variety of complications including pneumonia, collectively referred to as ventilator-associated events (VAEs) (3–6). The recent global pandemic of COVID-19, caused by SARS-CoV-2, has highlighted risks of ventilator treatment (7–11). Mechanical ventilation increases the risk of aspirating commensal bacteria into the lungs and use of sedation, particularly benzodiazepines or propofol, during ventilation is associated with an increased hazards ratio for VAEs (3–6).

The general anesthetic propofol has grown to become the predominant anesthetic in clinical use throughout the world, lauded for its rapid onset and offset, relatively mild side effects, and flexibility in both the induction and maintenance of anesthesia (12, 13). While there have been multiple reports on propofol's immunomodulatory effects *in vitro* (14–24), *in vivo* evidence has only recently begun to be reported. Klompas et al. correlated propofol sedation in mechanically-ventilated patients with a significantly increased risk of VAEs, including pneumonia, compared to patients not receiving propofol (5). Visvabharathy et al. reported that acute propofol sedation dramatically increased susceptibility to both *Listeria monocytogenes* and *Staphylococcus aureus* bloodstream infections in a mouse model and additionally led to more severe pathology at primary sites of infection (25, 26). This susceptibility correlated with a reduced capacity to effectively recruit mature immune effector cells to sites of infection following propofol sedation. These propofol-associated influences on host immunity are especially

important to pursue given that propofol is administered widely in both inpatient and outpatient procedures.

To explore the potential impact of propofol sedation on the outcome of respiratory infections, we have made use of a mouse model of lung infection with the opportunistic pathogen *Klebsiella pneumoniae (K. pneumoniae)*. *K. pneumoniae* is a gram-negative extracellular bacterium that is ubiquitous in the water and soil of the environment and also colonizes the nasopharynx and intestinal tract of humans and animals (27). It accounts for 3-8% of all nosocomial bacterial infections including pneumonia, Gram-negative bacteremia, and urinary tract infections (28). *K. pneumoniae* is the second most common cause of gram-negative bacteremia in the United States with 12-50% of *K. pneumoniae* bloodstream infections originating from the lungs (28–31). A significantly worse outcome of bacteremia is associated with *K pneumoniae* infections from a respiratory source (29). *K. pneumoniae* is a growing threat worldwide as a lethal nosocomial pathogen that is rapidly acquiring antimicrobial resistance (32).

Using an intranasal model of *K pneumoniae* infection in mice, we compared the impact of propofol versus ketamine/xylazine sedation on bacterial colonization of the lung, lung pathology, and the dissemination of bacteria to distal organs. We further investigated whether sedative choice influenced the requirement for distinct *K pneumoniae* virulence determinants using a whole genome insertion element (INSeq) approach.

MATERIALS AND METHODS

Bacterial media and strains. *K. pneumoniae* and *Escherichia coli* strains used in this study are listed in **Table 1**. Strains were grown at 37 °C in lysogeny broth (LB; per liter, 10 g Bacto-tryptone [BD], 5 g yeast extract [BD], 10 g NaCl [Sigma-Aldrich]). When cells were grown in the presence of hygromycin, low-salt LB was used (i.e., 5 g NaCl per liter). When necessary,

antibiotics (Gold Biotechnology) were added to the media at the following concentrations: rifampicin 30 µg ml^{-1}, hygromycin 100 µg ml^{-1}, kanamycin 50 µg ml^{-1}, and carbenicillin 100 µg ml^{-1}. When necessary, the following compounds were added to the media to the indicated final concentrations: sodium salicylate (Sigma-Aldrich): 2 mM; diaminopimelate (DAP; Sigma-Aldrich): 0.3 mM; arabinose (Gold Biotechnology): 100 mM. Growth media were solidified with 1.5% agar as needed. Standard molecular biology techniques were used to introduce plasmids into *E. coli* (i.e. electroporation) and into *K. pneumoniae* (i.e., electroporation or conjugation).

Animal infections. All animal procedures were approved by the University of Illinois Chicago Animal Care Committee and were conducted in the Biological Resources Laboratory. *K. pneumoniae* strains were cultured overnight, shaking (37°C, 180 rpm) in LB broth. The following morning, strains were subcultured 1:50 in fresh LB and incubated with shaking for one hour to an OD_{600} of 0.2-0.4. Optical density was adjusted to 0.2 OD_{600} with LB broth and bacteria were recovered by centrifugation, washed, and diluted to the desired CFU in sterile 1X phosphate-buffered saline (PBS) for infection. Strains were kept on ice until immediately before infection. Animals were sedated via tail vein injection with ketamine (20 mg/kg; Zoetis, Kalamazoo, MI) and xylazine (4 mg/kg; Akorn, Decatur, IL) in Intralipid as control or propofol (20 mg/kg; Zoetis) in Intralipid. For non-competitive infections, approximately 2.5 x 10^2 colony forming units (for propofol sedated mice) or 2.5 x 10^3 colony forming units (ketamine/xylazine sedated mice) of each strain was administered via intranasal route into 8- to 10-week old Swiss Webster mice (Envigo, Madison, WI) and for competitive infections, approximately 5 x 10^3 CFU of WT and a mutant were premixed and administered via intranasal route for a total 1 x 10^4 CFU dose. For non-competitive infections, mice were sacrificed after 24 or 48 hours. Lungs, livers, and spleens were isolated, homogenized, and plated in triplicate on LB agar containing rifampicin for enumeration of bacterial burdens in each organ. For competitive infections, mice were sacrificed

after 24 hours and lungs were homogenized and plated in triplicate on LB agar containing rifampicin and on LB agar containing rifampicin and kanamycin.

Histology. For histological analysis, mice were sacrificed via isoflurane (Henry Schein, Dublin, OH). The lung vasculature was perfused with 10 ml ice cold PBS containing 50U/ml heparin (Millipore Sigma, St. Louis, MO) to remove blood and lungs were infused with one milliliter of neutral buffered formalin solution (Millipore Sigma). Lungs were placed in 20 ml of neutral buffered formalin for 48 hours, then transferred into 70% ethanol. Paraffin-embedded sections were prepared by the UIC Research Histology and Tissue Imaging core facility. Five micron-thick sections were stained with hematoxylin and eosin (H&E) and mounted. Digital scans of H&E-stained lung sections were captured on a ScanScope CS and analyzed using ImageScope software (Aperio/Leica).

Immunofluorescence. For immunofluorescent analysis, mice were sacrificed via isoflurane. The lung vasculature was perfused with 10 ml ice cold PBS containing 50U/ml heparin to remove blood and lungs were infused with one milliliter of neutral buffered formalin solution (Millipore Sigma). Lungs were placed in 20 ml of neutral buffered formalin for 48 hours, then transferred into 70% ethanol. Unstained, paraffin-embedded sections of 5μm thickness were prepared by the UIC Research Histology and Tissue Imaging core facility. Paraffin was dissolved in xylenes and sections were rehydrated in graded ethanol washes, followed by washing in tris-buffered saline (TBS, pH 7.6). Antigen retrieval was carried out in 10 mM sodium citrate buffer with 0.05% Tween-20 (pH 6.0) in a pressure cooker on high temperature for fifteen minutes. Slides were blocked with Background Buster (Innovex, Richmond, CA). Primary antibody was *K. pneumoniae* rabbit polyclonal (ThermoFisher, Waltham, MA) and secondary antibody was goat anti-rabbit-FITC (Invitrogen, Carlsbad, CA). Slides were mounted with ProLong Gold antifade with DAPI (ThermoFisher), imaged using a Zeiss Axio Imager A2 upright

microscope (Carl Zeiss, Thornwood, NY), and analyzed on Zen 2012 (Carl Zeiss) imaging software.

Generation of KPPR1 transposon mutant library. KPPR1 and MJM2382 were grown overnight in LB and LB carb DAP, respectively, at 37 °C with aeration. Saturated cultures were diluted 1:80 in 3 ml and grown for 2 hours and 40 minutes at 37 °C. 2.5 ml of *E. coli* and 5 ml of *K. pneumoniae* were pelleted and combined in 500 µl LB, which was spotted in fifty 10-µl spots on LB. After 3.5 hours at 37 °C, each spot was swabbed into 500 µl LB, vortexed, and 50 µl was spread onto LB kan sal for overnight incubation at 37 °C (the presence of salicylic acid reduces the amount of capsule produced). An estimated 50,000 colonies were swabbed into 25 ml LB mixed with 12.5 ml 50% glycerol on ice and frozen at -80˚C with a final density of 3 x 10^{11} CFU/ml.

INSeq analysis. Genomic DNA was extracted using a Maxwell 16 instrument (Promega, Madison, WI). Transposon insertion junctions were amplified from three input samples and six output samples according to the previously published protocol (33). Samples were single-end sequenced with an Illumina HiSeq 2500 platform (Illumina, San Diego, CA) at the Tufts University Genomics Core Facility in Boston, MA with 45 million reads generated. FASTQ files were run through the pyinseq pipeline (https://github.com/mjmlab/pyinseq; v.0.2) using the KPPR1 complete genome sequence (34). The program demultiplexed the samples and organized the reads into the following categories: contig, nucleotide, Lcounts, Rcounts, totalCounts, cpm, threePrimeness, and locus_tag. The KPPR1 contig was CP009208.1 for all genes; the nucleotide position was the location of the transposon insertion; Lcount, Rcount and totalCount enumerated the sequences on either side of the transposon (with a roughly 50/50 percentage expected – hits with a skew greater than 1:10 were omitted); CPM (counts per million) was the total reads generated per individual transposon hit divided by 10^6;

threePrimeness was if the hit was present in an annotated gene and indicated where insertion fell between the start and stop codon; locus tag identified the name or position of the gene (represented by VK055_xxxx in KPPR1). The cpm counts of the three different biological replicates was first analyzed by the average value and then by the median, with the list of candidate genes sorted by the $\log_{10}$(output/input). Sequencing data were deposited at NCBI SRA under accessions SRR6480865-SRR6480873 as detailed in **Table S1**. A table of analyzed values for each KPPR1 gene is posted as **Table S2**.

Generation of *K. pneumoniae* gene deletion strains. Deletions were made in the KPPR1 background using Lambda Red recombination (35). Knockout cassettes for each gene were generated using the "KO" primers listed in **Table S3** to amplify the KanR cassette from pKD4 with homologous ends to chromosomal location of each gene. KPPR1 was electroporated with pACBSR-Hyg to create strain MJM2698. This strain was electroporated with each of the knockout cassettes. Strains with Kan resistance were selected and then patched onto low salt-LB-Hyg plates to confirm the loss of pACBSR-Hyg. Kan-resistant and Hyg-sensitive isolates were verified with PCR using the verification (V) primers listed in **Table S3**. The PCR product was submitted for Sanger sequencing at the Northwestern University Sanger Sequencing Core to confirm the integrity of the junctions where the knockout cassette replaced the gene of interest. To remove the KanR cassette, strains were electroporated with pFLP-Hyg and acquisition of the plasmid was selected on low salt-LB-Hyg media. Candidates were incubated at 42 ^{o}C overnight and then screened for loss of Kan resistance. Colonies that lost Kan resistance were passaged for several days on LB plates and then screened for Hyg sensitivity to confirm loss of pFLP-Hyg. PCR was used to confirm removal of the Kan cassette using the verification (V) primers listed in **Table S3**.

Construction of *K. pneumoniae* complementation strains. Complementation of deleted genes was accomplished by integrating wild-type alleles of the gene at the presumed neutral *att*Tn*7* chromosomal site using a site-specific Tn*7* transposon (**Figure S1**). Published vector pJMP1185 expresses a Cas9 system with a constitutive promoter driving expression of *mRFP* as a control (36). We first removed the *cas9* gene from the transposon to create pAD12. Primers AD_254 and AD_255 were used to amplify pJMP1185 without the *cas9* gene. The plasmid was ligated back together with T4 ligase and transformed into WM3064 *E. coli* cells. Candidates were selected on LB-Kan plates, plasmid insertion was verified with PCR using primers AD_191 and AD_192, and the correct sequence was confirmed with Nanopore sequencing (Plasmidsaurus). To generate complement vectors, the *mRFP* gene was replaced with one of the genes of interest to generate pAD14, pAD16, pAD18, or completely removed to generate an empty vector control (pAD12b). Primers AD_258 and AD_259 were used to amplify pAD12. The reaction was PCR purified and DpnI digested. Genes were amplified with either AD_264/AD_265, AD_272/AD_273, or AD_276/AD_277 and then cloned into the backbone using the NEB Hi-Fi assembly kit. For the empty vector control, primers DAT_535/DAT_536 were used to amplify the backbone and the Q5 site-directed mutagenesis kit (NEB) was used for assembly. For the complementation plasmids and empty vector control, the assembly mix was transformed into WM3064 *E. coli* cells and candidates were selected on LB-Kan. The resulting plasmids were verified with Nanopore sequencing (Plasmidsaurus). Plasmids were transformed into relevant *K. pneumoniae* strains using conjugation. Candidates were selected using Kan resistance and verified using PCR (DAT_529/DAT_530) and Nanopore sequencing (Plasmidsaurus).

***K. pneumoniae* growth assays**. To assess doubling time, strains were grown in LB broth at 37°C with shaking for three h, with samples taken every 30 min. Serial dilutions were spot plated to enumerate viable CFU and the doubling time was calculated from these points. To

assess growth on SDS/EDTA, cultures were grown to saturation in LB, serially diluted, and 5 µL was spotted on LB plates or LB plates containing 0.1% SDS/1.5 mM EDTA. Plates were incubated overnight at 37˚C and imaged with a Nikon D810 digital camera.

Statistical Analysis: For mouse experiments that compared multiple groups, bacterial burden data was log10 transformed and analyzed via the Kruskal Wallis test with Dunn's post-hoc test. For Western blot data analysis, after normalization, protein levels between conditions are compared via one-way ANOVA with Dunnetts post-hoc test. Relative RT-qPCR expression will be reported with normalization via the comparative C_T method (Schmittgen). ELISA and RT-qPCR experiments are also analyzed via one-way ANOVA. Data graphing and analysis was conducted on GraphPad Prism software.

RESULTS

Sedation with the anesthetic propofol leads to increased lung colonization with *K. pneumoniae*. Previous investigations into the impact of propofol on bloodstream infections using the Gram-positive pathogens *L. monocytogenes* and *S. aureus* revealed significant alterations in bacterial colonization, growth, and pathology in target organs (25). Given the prevalence of *K. pneumoniae* acquisition in health-care settings where propofol is widely used, and to examine the impact of propofol on a model Gram-negative pathogen, we assessed whether propofol affected lung infection of *K. pneumoniae* via an intra-nasal inoculation route. Female Swiss Webster mice were briefly sedated (5-10 minutes) with either propofol or ketamine/xylazine and intranasally infected with $3x10^4$ CFU KPPR1. Bacterial burdens were assessed at 24 and 48 hours post infection in the lung, liver, and spleen. Brief propofol sedation had no measurable impact on lung burdens 24 hours post-infection, but burdens were increased nearly 100-fold by 48 hours compared to ketamine/xylazine-sedated controls (**Figure 1A**). We also assessed the impact on dissemination from the lungs and again found that while secondary

organs had comparable burdens at 24 hours, average burdens in both livers and spleens were more than 1,000-fold higher than controls (**Figure 1B,C**). We conclude that the immunosuppressive phenotype observed with propofol sedation is broad enough to impact multiple routes of infection with both Gram-positive and Gram-negative bacteria.

Propofol exacerbates lung pathology associated with *K. pneumoniae* infection. Previous research on propofol sedation prior to infection identified gross changes in pathology at primary sites of infection (25, 26). When examining lung histology, we observed that by 72 hours post-infection, severe damage was widespread in lungs regardless of sedation agent (**Figure 2A-B**), however, propofol-sedated mouse lungs featured large areas of de-cellularized or denuded tissue containing little identifiable structure and only sporadic immune infiltration. Quantification of these regions showed that propofol-sedated mice contain significantly larger denuded regions within the lungs (**Figure 2C**). Immunofluorescent examination of these regions revealed that *K. pneumoniae* had completely overrun local containment and appeared to have developed a replicative niche (**Figure 2D**). It is likely that these bacteria-packed regions underlie the disparate burdens observed between sedation groups.

Transposon insertion sequencing identifies *K. pneumoniae* genes that are required for outgrowth in the lung in a sedative-dependent manner. Genome-wide approaches for the discovery of virulence factors required for *in vivo* growth have been applied in *K. pneumoniae* previously with considerable success (37–42). In addition to examining the impact of propofol on *K. pneumoniae* lung infection, we also sought to investigate what impact propofol might have on the *K. pneumoniae* global virulence repertoire required for successful growth in the lung. Transposon insertion sequencing (INSeq/Tn-seq) is a powerful, high resolution approach to analyze whole genomes by coupling Mariner transposon mutagenesis with high-throughput sequencing to rapidly and comprehensively quantify the relative fitness of large pools of

transposon mutants (43–45). We applied this approach by mutagenizing *K. pneumoniae* strain KPPR1, sedating mice with either propofol or ketamine/xylazine, followed by the infection of mice via the intranasal route. We generated a 50,000 mutant transposon library in KPPR1 using the plasmid pJNW684 (45). Hits were observed across the chromosome with an average of approximately 9.1 insertions per kb. We then used the experimental approach outlined in **Figure 3**. Three propofol-sedated and three ketamine/xylazine control-sedated mice were intranasally infected with the library at a dose of 6 x 10^5 CFU for 24 hours, after which the lungs were harvested and genomic DNA was extracted. The 24 h time point was selected to identify mutants that displayed fitness differences in advance of the lethality differences that begin to occur at 48 h with the use of a higher CFU dose and so that the analysis was not complicated by the high proportion of lethality at the later time point. The higher CFU dose of 6 x 10^5 CFU was selected to increase mutant representation within the library for the subsequent INSeq analyses. Genomic DNA was also extracted from aliquots of the input library grown under media conditions to mimic the number of generations for the lung output. In total, 4,250 genes contained insertions in our input pools (minimum 10 cpm in all replicates) with the top 770 genes representing 50% of all insertions. Interestingly, genes were identified as uniquely required for infection following sedation with either anesthetic (**Figure 3B**).

Relative fitness was calculated by taking the average number of output reads for each treatment, dividing by the average number of input reads, and taking the log of the quotient. To maximize the likelihood that a given mutant would accurately reflect its observed fitness defect(s), we imposed conservative statistical cutoffs. We excluded genes with less than median 20 cpm in the input pools, which narrowed the list of genes to 4,093, from which we identified candidates that differentially required following each sedative. We looked for genes that displayed at least a log10 difference between the two anesthetic conditions and minimal variation within a condition (typically CV<75%). The genes *copA (VK055_2084)* and *ilvC (VK055_3202)* were previously validated as genuinely defective in virulence and serve to

confirm the success of the screen (**Figure 4**) (46). The genes *virK* (VK055_0094/RS00455), *VK055_1993 (RS09970)*, and *glnB* (VK055_4623/RS23395) were identified as potentially only required following ketamine/xylazine sedation, while the genes *VK055_1398, VK055_3638 (RS18420), VK055_3462 (RS17525)*, and *fepC* (VK055_1930/ RS09665) were likely to be more important following propofol sedation. Additionally, we chose to investigate *mlaC (VK055_3875)* as it was identified as having a strong defect regardless of sedative choice and was representative of most of the *mla* genes (**Figure S2**).

Individual mutant and competitive infection experiments validate the global INSeq/Tn-seq analysis. To validate the global INSeq analysis, we conducted both individual mutant and competitive infection experiments. Deletions were made in the KPPR1 background using Lambda Red recombination. Eight genes yielding a variety of putative sedative-dependent (*ΔVK055_1993, ΔVK055_3462, ΔVK055_3638, ΔvirK, ΔglnB*, and *ΔVK055_1398*) and independent (*ΔmlaC* and *ΔfepC*) phenotypes were chosen. The desired genotypes were confirmed by diagnostic PCR and sequencing. Competition infections were performed using a 1:1 mixture of KPPR1 and single deletion mutants. Most of the gene candidates exhibited sedative-dependent phenotypes consistent with the original Tn mutant selection (**Figure 5**). This was observed for the *ΔmlaC, ΔglnB, ΔVK055_1398, ΔVK055_1993,* and *ΔVK055_1398* strains. However, *ΔvirK*, *ΔVK055_3462,* and *ΔVK055_3638* mutants yielded unexpected phenotypes in the direct competition experiment. *VK055_3462* was found dispensable for infection during both sedative conditions. While based on INSeq, the Δ*virK* mutant had a specific defect under ketamine/xylazine, the 1:1 competition resulted in a pronounced defect only during propofol sedation (**Figure 5**). Although distinct from the result from INSeq, this outcome provides an additional mutant by which to probe the requirement's function under propofol. *VK055_3638* in INSeq analysis had a specific defect under propofol, while the 1:1 competition resulted in a slight defect regardless of sedative choice.

Our screen identified mutants depleted selectively in either propofol or ketamine/xylazine sedation as well as mutants depleted under both sedative conditions. Identifying genes required broadly for *K. pneumoniae* lung colonization highlights virulence factors required irrespective of anesthetic choice. 327 genes were required in both sedative conditions (mutants >10-fold depleted), with Table 2 illustrating genes for which mutants exhibited >1,000-fold depletion in both conditions. Competitive infections identified *fepC*, *mlaC,* and *VK055_3638* as required for *K. pneumoniae* lung colonization following sedation by either propofol or ketamine (**Figure 5**). *In vitro* characterization of these mutants revealed all deletions demonstrated WT-like growth in broth, except for Δ*fepC,* which had a 16% increase in doubling time (20.92±0.55 min) compared to KPPR1 (18.07±0.34 min) (**Figure 6A**). Increased sensitivity to detergents, specifically a combination of SDS and EDTA (47) has been previously shown for *mla* genes in *E. coli*. The *K. pneumoniae* Δ*mlaC* mutant was similarly found to exhibit sensitivity to SDS and EDTA, a phenotype that can be reversed upon complementation with the wild-type *mlaC* expressed at the chromosomal *att*Tn*7* site (**Figure 6B**). The Δ*mlaC* strain was selected for further *in vivo* examination in individual infections based on its contributions to lung colonization following sedation under either propofol or ketamine/xylazine. The Δ*VK055_3638* mutant was also selected for further characterization based on its requirement during competitive infections with WT strains vs its apparent specific requirement following propofol sedation as indicated from the INSeq experiments. Δ*glnB* was selected for further study based on its specific requirement during ketamine/xylazine sedation.

Given that propofol sedation appeared to significantly enhance mouse susceptibility to *K. pneumoniae* infection, we identified an infectious dose for propofol sedated animals that enabled mouse survival for beyond 48 hours so as to provide a more extended time window for assessment of potential mutant phenotypes. An intravenous dose of 250 CFU of KPPR1 was found to establish robust and reproducible levels of infection despite being 10 to 100-fold lower than doses routinely reported in the literature (**Figure 7A**) (48–50). For the comparison of

propofol sedated animals with single infections under ketamine sedation, a ten-fold increase to the inoculum was required for animals sedated with ketamine to detect any difference between attenuated mutant strains and WT as animals rapidly cleared lower doses of WT *K. pneumoniae* (**Figure 7B**). The requirement for *mlaC* was validated for mono-infections under both sedative conditions and could be fully complemented by the introduction of *mlaC* at a distinct chromosomal location (**Figure 7B,C**). In contrast to competitive infections, the *glnB* deletion mutant was found to demonstrate a sedative-specific defect in virulence following propofol sedation instead of ketamine (**Figure 7B,D**). Also contrary to the results obtained using WT and mutant competitive infections, *VK055_3638* in mono-infections was not found to be significantly different from WT following sedation with either propofol or ketamine (**Figure 7B,E**). The differences observed for mutant phenotypes as defined by competition experiments versus mono-infection may reflect cross complementation of strains, differences in the overall bacterial load used for the INSeq and competition experiments, and/or the ability of either WT or mutant strains to influence host immune responses (discussed below). Overall, our results indicate important differences in the requirement for *K. pneumoniae* virulence factors based on the type of sedative used during mouse infection.

DISCUSSION

Previous work identified the significant impact of brief propofol exposure on the ability of an infected host to combat bacterial bloodstream infections with either *L. monocytogenes* or *S. aureus*, both Gram-positive bacterial pathogens (25, 26). Here, we have demonstrated that propofol's immunomodulatory phenotype is also relevant to both a new route of infection (intranasal) and to a Gram-negative pathogen, *K. pneumoniae*. Propofol sedation increased lung burdens approximately 100-fold compared to ketamine/xylazine-sedated mice and furthermore increased dissemination to secondary organs approximately 1,000-fold at 48 hours post-infection (**Figure 1**). We further identified that propofol sedation resulted in significantly

larger areas of denuded or destroyed lung tissue (**Figure 2**), likely forming a replicative niche for rapidly dividing *K. pneumoniae in vivo* and possibly accounting for the increased lung burdens measured at 48 hours post-infection. Serious disseminated infections also resulted from a low dose inoculum (200 CFU) indicating the increased susceptibility of propofol sedated mice to *K. pneumoniae* lung infection (**Figure 7**). These data clearly demonstrate that propofol negatively impacts the host's ability to address *K. pneumoniae* lung infection and subsequent bacteremia. Whether these changes in host immune responses resemble those previously reported for bacterial bloodstream infections, which included dramatic reductions in the populations of mature macrophages (25, 26) has not yet been determined. Lung histology indicates abundant immune cell infiltration into the infected lungs with evident differences in the resultant pathology (**Figure 2**).

Genome-wide mutagenic approaches such as signature-tagged mutagenesis (STM) and transposon mutagenesis have previously been applied as *K. pneumoniae in vivo* virulence screens and have identified dozens of putative virulence factors, which have been comprehensively reviewed by Paczosa and Mecsas (30). The screen described herein yielded novel gene products by considering sedative exposure as a key variable in subsequent lung outgrowth. By comparing outputs from infected lungs to their inputs, we were able to quantify the relative requirement of numerous genes following either ketamine/xylazine or propofol sedation. This approach enabled us to identify novel virulence determinants and begin to define the broad impact that sedation has on lung fitness. The choice of ketamine/xylazine for comparison was based both on the common use of this anesthetic/sedative in animal experiments, and because the drugs were previously shown to have minimal effects on the control of bloodstream bacterial infections (25, 26). Interestingly, clear effects on host immunity were also evident following ketamine/xylazine sedation, suggesting that sedative use in general may impact host immunity, albeit perhaps to different degrees. This finding is consistent with a

recent report from Gage et al indicating that ketamine sedation negatively impacted bacterial clearance and lung tissue pathology using a *Pseudomonas aeruginosa* pneumonia model (51).

Based on the results of the INSeq analysis, several *K. pneumoniae* mutants were selected for additional characterization. The *mla* (maintenance of outer membrane lipid asymmetry) pathway has been well characterized in *E. coli* (47). Mla comprises a transport system that shuttles phospholipids from the outer membrane to the inner membrane (47). MlaFEDB forms an ABC transporter, while MlaA is a lipoprotein attached to the outer membrane and MlaC is the periplasmic shuttle between the two. Loss of *mlaC* resulted in a significant defect under both sedative conditions (**Figure 7**). A direct comparison between propofol and ketamine/xylazine sedated animals for mutant phenotypes was somewhat constrained by the need to use increased CFU to establish infection in ketamine/xylazine sedated mice. Virulence defects similar to those observed for the *mlaC* mutant would be predicted for *mlaA*, mlaD, *mlaE*, and *mlaF* based on their representation in the INSeq screen (**Figure S2**). In contrast, the loss of *mlaB* does not appear to carry a significant defect based on the INSeq results, a reasonable finding considering that MlaB is a minor subunit in the transporter. *mlaA* has been recently confirmed as a virulence requirement for *K. pneumoniae* lung infections in mice (52). The perturbation of membrane lipid homeostatic mechanism is therefore likely a critical factor in the resistance of *K. pneumoniae* to host antimicrobial strategies, and this host defense may be somehow enhanced by propofol exposure, resulting in enhanced clearance of *mlaC* mutants.

Competition infections predicted a general virulence defect for Δ*VK055_3638* mutants under both sedative conditions. However, mono-culture lung infections indicated no significant decline in mutant fitness following either propofol or ketamine/xylazine sedation. *VK055_3638* is an uncharacterized putative membrane protein of 91 amino acids. Our results suggest that mutants lacking *VK055_3638* are outcompeted by WT bacteria during mixed infections, but the overall defect in virulence appears modest based on the ability of mutants to colonize the

mouse lung in the absence of bacterial competitors. A defined role for *VK055_3638* awaits a better understanding of the function of this predicted membrane protein.

Of the four genes demonstrating differential competitive defects (*VK055_1993*, *virK*, *glnB*, and *VK055_1398*), only *glnB* has been previously characterized, while the other three remain annotated as unknown or hypothetical. *glnB* encodes P_{II}, a regulator of glutamine synthetase (GS). This protein effectively senses the nitrogen status of the bacterium through allosteric regulation by α-ketoglutarate and glutamine (53, 54). High intracellular glutamine levels cause P_{II} to adenylylate GS, effectively turning it off, while α-ketoglutarate binding to P_{II} leads to de-adenylylation of GS and its activation. Interestingly, while the Δ*glnB* mutant appeared defective under ketamine/xylazine sedation in mixed infections but not in propofol sedated mice (**Figure 5A**), this phenotype was reversed for mono-culture infections (**Figure 7**). The differential requirement under for mixed infections under ketamine/xylazine sedation was also noted, although not confirmed, for the gene *glnS* (VK055_1830/RS09165), encoding glutamine-tRNA ligase, but not in any of the other six *gln* family genes. Metabolic modeling has found that KPPR1 can utilize a diverse array of nitrogen sources (55, 56) and it is possible that there are both sedation-dependent and strain-induced shifts in host nitrogen metabolism that might explain the varying requirement for *glnB*.

Our dataset suggests numerous other genes that are potentially differentially required depending on host anesthetic exposure. Further validation and characterization of these gene products is needed to provide clarity to these findings. While the results presented support a growing body of evidence that indicates that the choice of sedative used for anesthesia can profoundly influence the course of bacterial infection, our work goes on to show that the virulence gene repertoire required for infection differs dependent upon sedative choice. This finding has important implications for the selection of potential new drug targets for *K. pneumoniae* infections; the most effective targets are likely to be those gene products that are required regardless of the type of sedation that may be used. Taken together, these results

reveal that propofol sedation leads to the exacerbation of lung infections caused by the bacterial pathogen *K. pneumoniae.* Future studies aimed towards identifying colonization and virulence factors required under multiple sedation conditions should clarify which aspects of host immunity are negatively impacted by sedative exposure, and what steps might be taken to reverse immune suppression during sedation.

ACKNOWLEDGMENTS

We thank Alan Hauser and Nengding (Julie) Wang for plasmid pJNW684 and use of the Promega Maxwell instrument, Jason Peters for pJMP1185 and advice on modifying the plasmid, and Emanuel Burgos for computational assistance. This work was supported by the Chicago Biomedical Consortium Catalyst Award (to M.J.M. and N.E.F.), NIH grant R21AI166098 (to N.E.F. and M.J.M.), and NIH grant R35GM148385 (to M.J.M.). Its contents are solely the responsibility of the authors and do not necessarily represent the official views of the funding source.

Table 1. Bacterial strain and plasmid list.

Strain	Relevant Genotype	Reference
K. pneumoniae		
MJM2383	KPPR1	(34)
MJM2402	Transposon mutant library in KPPR1	This study
MJM2698	MJM2383 pACBSR-Hyg	This study
MJM2793	KPPR1 Δ*VK055_3462*::*kan*	This study
MJM2794	KPPR1 Δ*VK055_1993*::*kan*	This study
MJM2795	KPPR1 Δ*virK*(*VK055_0094*)::*kan*	This study
MJM2796	KPPR1 Δ*fepC*(*VK055_1930*)::*kan*	This study
MJM2797	KPPR1 Δ*mlaC*(*VK055_3875*)::*kan*	This study
MJM2784	KPPR1 Δ*glnB*(*VK055_4623*)::*kan*	This study
MJM2816	KPPR1 Δ*VK055_3638*::*kan*	This study
MJM3001	KPPR1 Δ*VK055_1398*::*kan*	This study
MJM3079	KPPR1 Δ*VK055_3638*	This study
MJM5801	KPPR1 Δ*glnB*	This study
MJM5804	KPPR1 Δ*mlaC*	This study
MJM5821	KPPR1 Δ*VK055_3638 att*Tn*7*::*VK055_3638*	This study
MJM5823	KPPR1 Δ*fepC att*Tn*7*::*fepC*	This study
MJM6053	KPPR1 Δ*mlaC att*Tn*7*::*mlaC*	This study
MJM6260	KPPR1 *att*Tn*7*::*kan*	This study
MJM6261	KPPR1 ΔVK055_3638 *att*Tn*7*::*kan*	This study
MJM6262	KPPR1 Δ*glnB att*Tn*7*::*kan*	This study
MJM6264	KPPR1 Δ*mlaC att*Tn*7*::*kan*	This study
E. coli		
MJM537	DH5α λpir	(57)
MJM1424 (β3914)	F- RP4-2-Tc::Mu Δ*dapA*::(erm-pir) *gyrA*462 zei-298::Tn10 (ErmR KanR TetR)	(58)
MJM2382	MJM1424 pJNW684	(45)
MJM534	CC118 λpir / pEVS104	(59)
MJM1649	BW25141 / pKD4	(60)
MJM2532	MJM1424 pACBSR-Hyg	This study
MJM2369	pFLP-Hyg	(35)
MJM4078	WM6026 dap-, pir+, attTn7::acrIIA4, recA1, dapA::pir / pJMP1039	(61)
MJM4080	WM6026 dap-, pir+, attTn7::acrIIA4, recA1, dapA::pir / pJMP1185	(61)
MJM5331 (WM3064)	*thrB1004 pro thi rpsL hsdS lacZ*ΔM15 RP4-1360 Δ(*araBAD*)567 Δ*dapA1341*::[*erm pir*]	(62)
MJM5713	WM3064 λpir / pAD12	This study
MJM5749	WM3064 λpir / pAD14	This study
MJM5751	WM3064 λpir / pAD16	This study
MJM5851	WM3064 λpir / pAD18	This study
MJM6259	WM3064 λpir / pAD12b	This study

Plasmids	Genotype/Description	
pJNW684	Transposon vector	(45)
pKD4	*FRT-kan-FRT* template	(60)
pACBSR-Hyg	Lambda-Red genes	(35)
pFLP-Hyg	FLP recombinase	(35)
pJMP1039	Helper for transposon on pJMP1185	(61)
pJMP1185	Transposon vector containing *cas9* system	(61)
pAD12	pJMP1185 without *cas9*	This study
pAD12b	pAD12 without *mRFP*	This study
pAD14	pAD12 with *VK055_3638*	This study
pAD16	pAD12 with *glnB*	This study
pAD18	pAD12 with *mlaC*	This study

Table 2. Genes for which mutants exhibited the highest shared fitness (depletion > 3 x 10^3) upon intranasal infection in both ketamine/xylazine and propofol.

		Fitness = Log_{10}(mouse output/culture input)	
Locus Tag	**Gene**	**Ketamine**	**Propofol**
VK055_3852	*gltD*	-3.65	-3.23
VK055_1782	*tolB*	-3.61	-3.60
VK055_3502	-	-3.51	-3.35
VK055_1783	*tolA*	-3.36	-3.36
VK055_2588	*serB*	-3.36	-3.20
VK055_4896	-	-3.30	-3.15
VK055_4025	*tolC*	-3.28	-3.12
VK055_4686	*purM*	-3.27	-3.27
VK055_1194	*trpD*	-3.24	-3.37
VK055_3504	-	-3.23	-3.37
VK055_1193	*trpE*	-3.23	-3.15
VK055_3499	-	-3.22	-3.36
VK055_3505	-	-3.21	-3.21
VK055_3088	*purD*	-3.20	-3.33
VK055_4578	-	-3.20	-3.33
VK055_5039	*hisF*	-3.19	-3.19
VK055_3728	-	-3.18	-3.18
VK055_2794	*pepA*	-3.13	-3.02
VK055_0991	*manA*	-3.12	-3.12
VK055_1196	*trpB*	-3.12	-3.41
VK055_5042	-	-3.08	-3.21
VK055_4685	*purN*	-3.04	-3.18
VK055_1785	*tolQ*	-3.02	-3.02

Supplemental Tables S1-S3:

- **Table S1. NCBI SRA Accession numbers.** Data deposition for the INSeq samples.
- **Table S2. INSeq data analysis for all samples.** Shown are counts-per-million (cpm) per gene for each sample from the pyinseq pipeline.

- **Table S3. Primer list.** Primers used for PCR during construction (P), or for verification by PCR and/or Sanger sequencing to verify insertion/orientation.

FIGURE LEGENDS

Figure 1. Brief propofol sedation increases *Klebsiella* lung burdens and dissemination to secondary tissues. Swiss Webster mice were sedated with either ketamine/xylazine (closed circles) or propofol (open circles) and infected with $3x10^4$ CFU intra-nasally and (A) lung, (B) liver, and (C) spleen burdens were assessed at 24 and 48 hours post infection. Statistics were calculated using the Mann Whitney U test (*, $p \leq 0.05$; **, $p \leq 0.01$).

Figure 2. Histological analysis of *K. pneumoniae* lung pathology 72 hours post-infection. Swiss Webster mice (n = 3 per group) were infected with $1x10^4$ CFU KPPR1. (A and B) After 72 hours, mice were euthanized and lungs harvested and processed for histological analysis. Representative H&E staining of ketamine/xylazine-sedated (A) and propofol-sedated (B) animals. Black bar = 100 µm. (C) Quantification of average denuded area in lung sections from 10 fields per mouse (n=3 per treatment). Statistics were calculated using an unpaired, two-tailed Student's t-test (**, $p \leq 0.01$). (D) Immunofluorescent staining of *K. pneumoniae* (red) in lung tissue (blue, DAPI).

Figure 3. Identification of novel *K. pneumoniae* virulence factors influenced by sedation using INSeq. (A) The colored rods symbolize separate mutants from a 50,000 transposon-mutant INSeq library in *K. pneumoniae* strain KPPR1. The dotted rods represent mutants that are expected to be absent after each selection. Examples are shown for mutants that exhibit (1) a growth defect; (2) inability to colonize ketamine/xylazine sedated mice but capable of colonization following propofol sedation; and (3) inability to colonize either ketamine/xylazine or propofol-sedated mice. (B) Identification of mutants required for lung colonization following propofol or ketamine/xylazine sedation. The X axis represents the approximately 5000 genes of the *K. pneumoniae* genome while the Y axis shows the difference of the median log ratio

following ketamine minus propofol sedation. The blue box indicates mutants less prevalent in the lungs of ketamine/xylazine sedated mice while the pink box indicates mutants less prevalent in the lungs of propofol sedated mice.

Figure 4. Potential competitive defects identified by INSeq. Competitive results for the input (circles), control-treated mice (squares), and propofol-treated mice (triangles). The values are normalized to the median of the three inputs. A) The first graph contains an example of a gene not relevant for virulence (*VK055_4268*) in either sedative condition. B) The remaining three graphs in the first row show genes with defects regardless of sedative used. Genes *copA* and *ilvC* were previously validated. *mlaC* is a general virulence factor. C) The second row (*virK, VK055_1993, glnB*) are genes for which mutants exhibited defects in ketamine-sedated mice only. D) Third row (*VK055_1398, fepC, VK055_3638, VK055_3462*) are genes for which mutants exhibited defects in propofol-sedated mice. Points in gray had zero normalized read counts and were set to 0.1 for the purpose of calculating log fold change.

Figure 5. Competitive infections with in-frame deletion mutants. Competitive indices of each mutant against WT 24 hours post-infection (n=4 per group). Mice were infected with approximately 5 x 10^3 CFU of WT and a mutant strain that were premixed and administered via intranasal route for a total 1 x 10^4 CFU dose. Statistics on lung titers were calculated using an unpaired, two-tailed Student's T-test.

Figure 6. Analysis of *in vitro* phenotypes of in-frame deletion mutants. (A) Deletion mutants were grown in LB broth at 37°C with shaking for three hours, with samples taken every 30 minutes. Serial dilutions were spot plated to enumerate viable CFU and the doubling time was calculated from these points. The data are representative of 3-5 independent experiments. (B) Saturated cultures were serially diluted and spotted onto specified media types, then grown

at 37°C overnight. The growth defect of the *mlaC* mutant on SDS/EDTA is able to be complemented.

Figure 7. Multiple mutants demonstrate competitive and non-competitive defects in a sedative-dependent manner. (A) Female Swiss Webster mice were sedated with 20mg/kg propofol or ketamine/xylazine and infected intranasally with 250 CFU KPPR1. Bacterial burdens assessed at 48 hours post-infection. The dotted line represents the limit of detection. p=.0219, One way ANOVA, Kruskal-Wallis posttest. (B-D) Female Swiss Webster mice (n=8-9 per group) were ketamine/xylazine sedated or propofol-sedated and infected with 2500 CFU (ketamine/xylazine sedated mice) or 250 CFU (propofol sedated mice) intranasally. The increased inoculum size for ketamine/xylazine sedated animals was necessary as mice cleared the infections at the lower (250 CFU) inoculum dose. Statistics were calculated using a two-tailed Mann-Whitney U test (*, $p \leq 0.05$; **, $p \leq 0.01$; ***, $p \leq 0.001$) and significance is compared to KPPR1 under the same sedative.

Figure S1. Tn*7* complementation approach.

(A) The *cas9* gene was removed from pJM1185 to create plasmid pAD12. Since this plasmid expresses *mRFP*, we used it to test expression levels in KPPR1 by confirming red fluorescence as seen in panel B. To create complemented strains, the genes were cloned in to replace the *mRFP* gene creating plasmids pAD14, pAD16, and pAD18 depending on the gene inserted. To create an empty vector control, *mRFP* was removed to create plasmid pAD12b. (B) From overnight growth in LB, 8 µl culture was spotted onto LB and grown for 24 h at 30 °C before imaging.

Figure S2. Potential *mla* operon defects identified by INSeq.

INSeq Competitive results for the input (circles), control-treated mice (squares), and propofol-treated mice (triangles). The values are normalized to the median of the three inputs. Points in gray had zero normalized read counts and were set to 0.1 for the purpose of calculating log fold change.

REFERENCES

1. Tablan OC, Anderson LJ, Besser R, Bridges C, Hajjeh R. 2004. Guidelines for preventing healthcare-associated pneumonia, 2003. MMWR Recomm Rep 53:1–36.

2. Patel SB, Kress JP. 2012. Sedation and analgesia in the mechanically ventilated patient. Am J Respir Crit Care Med 185:486–497.

3. Caroff DA, Szumita PM, Klompas M. 2016. The relationship between sedatives, sedative strategy, and healthcare-associated infection: A systematic review. Infect Control Hosp Epidemiol 37:1234–1242.

4. Klompas M. 2019. Ventilator-associated events: What they are and what they are not. Respir Care 64:953–961.

5. Klompas M, Li L, Szumita P, Kleinman K, Murphy MV, CDC Prevention Epicenters Program. 2016. Associations between different sedatives and ventilator-associated events, length of stay, and mortality in patients who were mechanically ventilated. Chest 149:1373–1379.

6. de Irala Estévez J, Fernández-Crehuet Navajas R, Díaz Molina C, Martínez de la Concha D, Salcedo Leal I, Masa Calles J. 1997. Risk factors for pneumonia, bacteremia, and urinary tract infection in an intensive care unit. Med Clin (Barc) 109:733–737.

7. Velly L, Gayat E, Quintard H, Weiss E, De Jong A, Cuvillon P, Audibert G, Amour J, Beaussier M, Biais M, Bloc S, Bonnet MP, Bouzat P, Brezac G, Dahyot-Fizelier C, Dahmani S, de Queiroz M, Di Maria S, Ecoffey C, Futier E, Geeraerts T, Jaber H, Heyer L, Hoteit R, Joannes-Boyau O, Kern D, Langeron O, Lasocki S, Launey Y, le Saché F, Lukaszewicz AC, Maurice-Szamburski A, Mayeur N, Michel F, Minville V, Mirek S, Montravers P, Morau E, Muller L, Muret J, Nouette-Gaulain K, Orban JC, Orliaguet G, Perrigault PF, Plantet F, Pottecher J, Quesnel C, Reubrecht V, Rozec B, Tavernier B, Veber B, Veyckmans F, Charbonneau H, Constant I, Frasca D, Fischer M-O, Huraux C, Blet A, Garnier M. 2020. Guidelines: Anaesthesia in the context of COVID-19 pandemic. Anaesth Crit Care Pain Med 39:395–415.

8. Yamamoto K. 2020. Risk of propofol use for sedation in COVID-19 patient. Anaesthesiol Intensive Ther 52:354–355.

9. Hirota K, Lambert DG. 2020. Propofol and SARS-CoV-2 infection. Br J Anaesth 125:e475–e476.

10. Babu VK, Rojas P, Perez Del Nogal G, Garcia-Fernandez A. 2023. Unusual case of propofol-related infusion syndrome complicating severe COVID-19 ARDS. BMJ Case Rep 16:e249456.

11. Koutsogiannaki S, Bu W, Maisat W, Manzor M, Zhang Z, Ohto U, Eckenhoff RG, Yuki K. 2022. Propofol directly binds to and inhibits TLR7. FASEB J 36:e22481.

12. Vasileiou I, Xanthos T, Koudouna E, Perrea D, Klonaris C, Katsargyris A, Papadimitriou L. 2009. Propofol: a review of its non-anaesthetic effects. Eur J Pharmacol 605:1–8.

13. Darnobid JA. 2015. The pharmacology of total intravenous anesthesia. Int Anesthesiol Clin 53:13–27.

14. Mikawa K, Akamatsu H, Nishina K, Shiga M, Maekawa N, Obara H, Niwa Y. 1998. Propofol inhibits human neutrophil functions. Anesth Analg 87:695–700.

15. Chen R-M, Wu C-H, Chang H-C, Wu G-J, Lin Y-L, Sheu J-R, Chen T-L. 2003. Propofol suppresses macrophage functions and modulates mitochondrial membrane potential and cellular adenosine triphosphate synthesis. Anesthesiology 98:1178–1185.

16. Fourcade O, Simon M-F, Litt L, Samii K, Chap H. 2004. Propofol inhibits human platelet aggregation induced by proinflammatory lipid mediators. Anesth Analg 99:393–398.

17. Hsing C-H, Lin M-C, Choi P-C, Huang W-C, Kai J-I, Tsai C-C, Cheng Y-L, Hsieh C-Y, Wang C-Y, Chang Y-P, Chen Y-H, Chen C-L, Lin C-F. 2011. Anesthetic propofol reduces endotoxic inflammation by inhibiting reactive oxygen species-regulated Akt/IKKβ/NF-κB signaling. PLoS One 6:e17598.

18. Jawan B, Kao Y-H, Goto S, Pan M-C, Lin Y-C, Hsu L-W, Nakano T, Lai C-Y, Sun C-K, Cheng Y-F, Tai M-H, Eng H-L, Wang C-S, Huang C-J, Lin C-R, Chen C-L. 2008. Propofol pretreatment attenuates LPS-induced granulocyte-macrophage colony-stimulating factor production in cultured hepatocytes by suppressing MAPK/ERK activity and NF-κB translocation. Toxicol Appl Pharmacol 229:362–373.

19. Inada T, Kubo K, Ueshima H, Shingu K. 2011. Intravenous anesthetic propofol suppresses prostaglandin E2 production in murine dendritic cells. J Immunotoxicol 8:359–366.

20. Meng T, Yu J, Lei Z, Wu J, Wang S, Bo Q, Zhang X, Ma Z, Yu J. 2013. Propofol reduces lipopolysaccharide-induced, NADPH oxidase (NOX 2) mediated TNF- α and IL-6 production in macrophages. Clin Dev Immunol 2013:325481.

21. Ren X, Lv F, Fang B, Liu S, Lv H, He G, Ma H, Cao Y, Wang Y. 2014. Anesthetic agent propofol inhibits myeloid differentiation factor 88-dependent and independent signaling and mitigates lipopolysaccharide-mediated reactive oxygen species production in human neutrophils in vitro. Eur J Pharmacol 744:164–172.

22. Inada T, Hirota K, Shingu K. 2015. Intravenous anesthetic propofol suppresses prostaglandin E2 and cysteinyl leukotriene production and reduces edema formation in arachidonic acid-induced ear inflammation. J Immunotoxicol 12:261–265.

23. Li S, Wang C-X, Liu N-Z, Liu P. 2015. Anti-inflammatory effects of propofol on lipopolysaccharides-treated rat hepatic Kupffer cells. Cell Biochem Biophys 71:845–850.

24. Okuno T, Koutsogiannaki S, Ohba M, Chamberlain M, Bu W, Lin F-Y, Eckenhoff RG, Yokomizo T, Yuki K. 2017. Intravenous anesthetic propofol binds to 5-lipoxygenase and

attenuates leukotriene B4 production. FASEB J 31:1584–1594.

25. Visvabharathy L, Freitag NE. 2017. Propofol sedation exacerbates kidney pathology and dissemination of bacteria during *Staphylococcus aureus* bloodstream infections. Infect Immun 85:10.1128/iai.00097-17.

26. Visvabharathy L, Xayarath B, Weinberg G, Shilling RA, Freitag NE. 2015. Propofol increases host susceptibility to microbial infection by reducing subpopulations of mature immune effector cells at sites of infection. PLoS One 10:e0138043.

27. Dai P, Hu D. 2022. The making of hypervirulent *Klebsiella pneumoniae*. J Clin Lab Anal 36:e24743.

28. Ashurst JV, Dawson A. 2025. Klebsiella pneumonia. StatPearls. StatPearls Publishing, Treasure Island (FL).

29. Al-Hasan MN, Lahr BD, Eckel-Passow JE, Baddour LM. 2010. Epidemiology and outcome of *Klebsiella* species bloodstream infection: a population-based study. Mayo Clin Proc 85:139–144.

30. Paczosa MK, Mecsas J. 2016. *Klebsiella pneumoniae*: Going on the Offense with a Strong Defense. Microbiol Mol Biol Rev 80:629–661.

31. Holmes CL, Wilcox AE, Forsyth V, Smith SN, Moricz BS, Unverdorben LV, Mason S, Wu W, Zhao L, Mobley HLT, Bachman MA. 2023. *Klebsiella pneumoniae* causes bacteremia using factors that mediate tissue-specific fitness and resistance to oxidative stress. PLoS Pathog 19:e1011233.

32. Wyres KL, Holt KE. 2016. *Klebsiella pneumoniae* Population Genomics and Antimicrobial-Resistant Clones. Trends Microbiol 24:944–956.

33. Goodman AL, Wu M, Gordon JI. 2011. Identifying microbial fitness determinants by insertion sequencing using genome-wide transposon mutant libraries. Nat Protoc 6:1969–1980.

34. Broberg CA, Wu W, Cavalcoli JD, Miller VL, Bachman MA. 2014. Complete genome sequence of *Klebsiella pneumoniae* strain ATCC 43816 KPPR1, a rifampin-resistant mutant commonly used in animal, genetic, and molecular biology studies. Genome Announc 2:e00924-14.

35. Huang T-W, Lam I, Chang H-Y, Tsai S-F, Palsson BO, Charusanti P. 2014. Capsule deletion via a λ-Red knockout system perturbs biofilm formation and fimbriae expression in *Klebsiella pneumoniae* MGH 78578. BMC Res Notes 7:13.

36. Banta AB, Ward RD, Tran JS, Bacon EE, Peters JM. 2020. Programmable gene knockdown in diverse bacteria using mobile-CRISPRi. Curr Protoc Microbiol 59:e130.

37. Maroncle N, Balestrino D, Rich C, Forestier C. 2002. Identification of *Klebsiella pneumoniae* genes involved in intestinal colonization and adhesion using signature-

tagged mutagenesis. Infect Immun 70:4729–4734.

38. Struve C, Forestier C, Krogfelt KA. 2003. Application of a novel multi-screening signature-tagged mutagenesis assay for identification of *Klebsiella pneumoniae* genes essential in colonization and infection. Microbiology 149:167–176.

39. Lawlor MS, Hsu J, Rick PD, Miller VL. 2005. Identification of *Klebsiella pneumoniae* virulence determinants using an intranasal infection model. Mol Microbiol 58:1054–1073.

40. Lau HY, Clegg S, Moore TA. 2007. Identification of *Klebsiella pneumoniae* genes uniquely expressed in a strain virulent using a murine model of bacterial pneumonia. Microb Pathog 42:148–155.

41. Tu Y-C, Lu M-C, Chiang M-K, Huang S-P, Peng H-L, Chang H-Y, Jan M-S, Lai Y-C. 2009. Genetic requirements for *Klebsiella pneumoniae*-induced liver abscess in an oral infection model. Infect Immun 77:2657–2671.

42. Silver RJ, Paczosa MK, McCabe AL, Balada-Llasat J-M, Baleja JD, Mecsas J. 2019. Amino acid biosynthetic pathways are required for *Klebsiella pneumoniae* growth in immunocompromised lungs and are druggable targets during infection. Antimicrob Agents Chemother 63:e02674-18.

43. Goodman AL, McNulty NP, Zhao Y, Leip D, Mitra RD, Lozupone CA, Knight R, Gordon JI. 2009. Identifying genetic determinants needed to establish a human gut symbiont in its habitat. Cell Host Microbe 6:279–289.

44. Brooks JF 2nd, Gyllborg MC, Cronin DC, Quillin SJ, Mallama CA, Foxall R, Whistler C, Goodman AL, Mandel MJ. 2014. Global discovery of colonization determinants in the squid symbiont *Vibrio fischeri*. Proc Natl Acad Sci U S A 111:17284–17289.

45. Wang N, Ozer EA, Mandel MJ, Hauser AR. 2014. Genome-wide identification of *Acinetobacter baumannii* genes necessary for persistence in the lung. mBio 5:e01163-14.

46. Bachman MA, Breen P, Deornellas V, Mu Q, Zhao L, Wu W, Cavalcoli JD, Mobley HLT. 2015. Genome-wide identification of *Klebsiella pneumoniae* fitness genes during lung infection. MBio 6:e00775.

47. Malinverni JC, Silhavy TJ. 2009. An ABC transport system that maintains lipid asymmetry in the gram-negative outer membrane. Proc Natl Acad Sci U S A 106:8009–8014.

48. Bachman MA, Oyler JE, Burns SH, Caza M, Lépine F, Dozois CM, Weiser JN. 2011. *Klebsiella pneumoniae* yersiniabactin promotes respiratory tract infection through evasion of lipocalin 2. Infect Immun 79:3309–3316.

49. Vornhagen J, Sun Y, Breen P, Forsyth V, Zhao L, Mobley HLT, Bachman MA. 2019. The *Klebsiella pneumoniae* citrate synthase gene, *gltA*, influences site specific fitness during infection. PLoS Pathog 15:e1008010.

50. Walker KA, Miner TA, Palacios M, Trzilova D, Frederick DR, Broberg CA, Sepúlveda VE, Quinn JD, Miller VL. 2019. A *Klebsiella pneumoniae* regulatory mutant has reduced capsule expression but retains hypermucoviscosity. MBio 10.

51. Gage H, Hannah SM, Hancock B, Cornax I, Munguia J, Olson J, Bjånes E, Zurich R, Hoffman A, Askarian F, Tong K, Liu L, Nizet V, Meier A. 2025. Anesthetic choice impacts mortality and bacterial clearance in a murine experimental pneumonia model. BMC Infect Dis 25:1–10.

52. Wu K, Lin X, Lu Y, Dong R, Jiang H, Svensson SL, Zheng J, Shen N, Camilli A, Chao Y. 2024. RNA interactome of hypervirulent *Klebsiella pneumoniae* reveals a small RNA inhibitor of capsular mucoviscosity and virulence. Nat Commun 15:6946.

53. Holtel A, Merrick MJ. 1989. The *Klebsiella pneumoniae* PII protein (*glnB* gene product) is not absolutely required for nitrogen regulation and is not involved in NifL-mediated *nif* gene regulation. Mol Gen Genet 217:474–480.

54. Leonardo JM, Goldberg RB. 1980. Regulation of nitrogen metabolism in glutamine auxotrophs of *Klebsiella pneumoniae*. J Bacteriol 142:99–110.

55. Henry CS, Rotman E, Lathem WW, Tyo KEJ, Hauser AR, Mandel MJ. 2017. Generation and Validation of the iKp1289 Metabolic Model for *Klebsiella pneumoniae* KPPR1. J Infect Dis 215:S37–S43.

56. Vezina B, Watts SC, Hawkey J, Cooper HB, Judd LM, Jenney AWJ, Monk JM, Holt KE, Wyres KL. 2023. Bactabolize: A tool for high-throughput generation of bacterial strain-specific metabolic models. eLife.

57. Brooks JF 2nd, Gyllborg MC, Kocher AA, Markey LEH, Mandel MJ. 2015. TfoX-based genetic mapping identifies *Vibrio fischeri* strain-level differences and reveals a common lineage of laboratory strains. J Bacteriol 197:1065–1074.

58. Le Roux F, Binesse J, Saulnier D, Mazel D. 2007. Construction of a Vibrio splendidus mutant lacking the metalloprotease gene vsm by use of a novel counterselectable suicide vector. Appl Environ Microbiol 73:777–784.

59. Stabb EV, Ruby EG. 2002. RP4-based plasmids for conjugation between *Escherichia coli* and members of the *Vibrionaceae*. Methods Enzymol 358:413–426.

60. Datsenko KA, Wanner BL. 2000. One-step inactivation of chromosomal genes in *Escherichia coli* K-12 using PCR products. Proc Natl Acad Sci U S A 97:6640–6645.

61. Peters JM, Koo B-M, Patino R, Heussler GE, Hearne CC, Qu J, Inclan YF, Hawkins JS, Lu CHS, Silvis MR, Harden MM, Osadnik H, Peters JE, Engel JN, Dutton RJ, Grossman AD, Gross CA, Rosenberg OS. 2019. Enabling genetic analysis of diverse bacteria with Mobile-CRISPRi. Nat Microbiol 4:244–250.

62. Wang P, Yu Z, Li B, Cai X, Zeng Z, Chen X, Wang X. 2015. Development of an efficient conjugation-based genetic manipulation system for *Pseudoalteromonas*. Microb Cell

781 Fact 14:11.

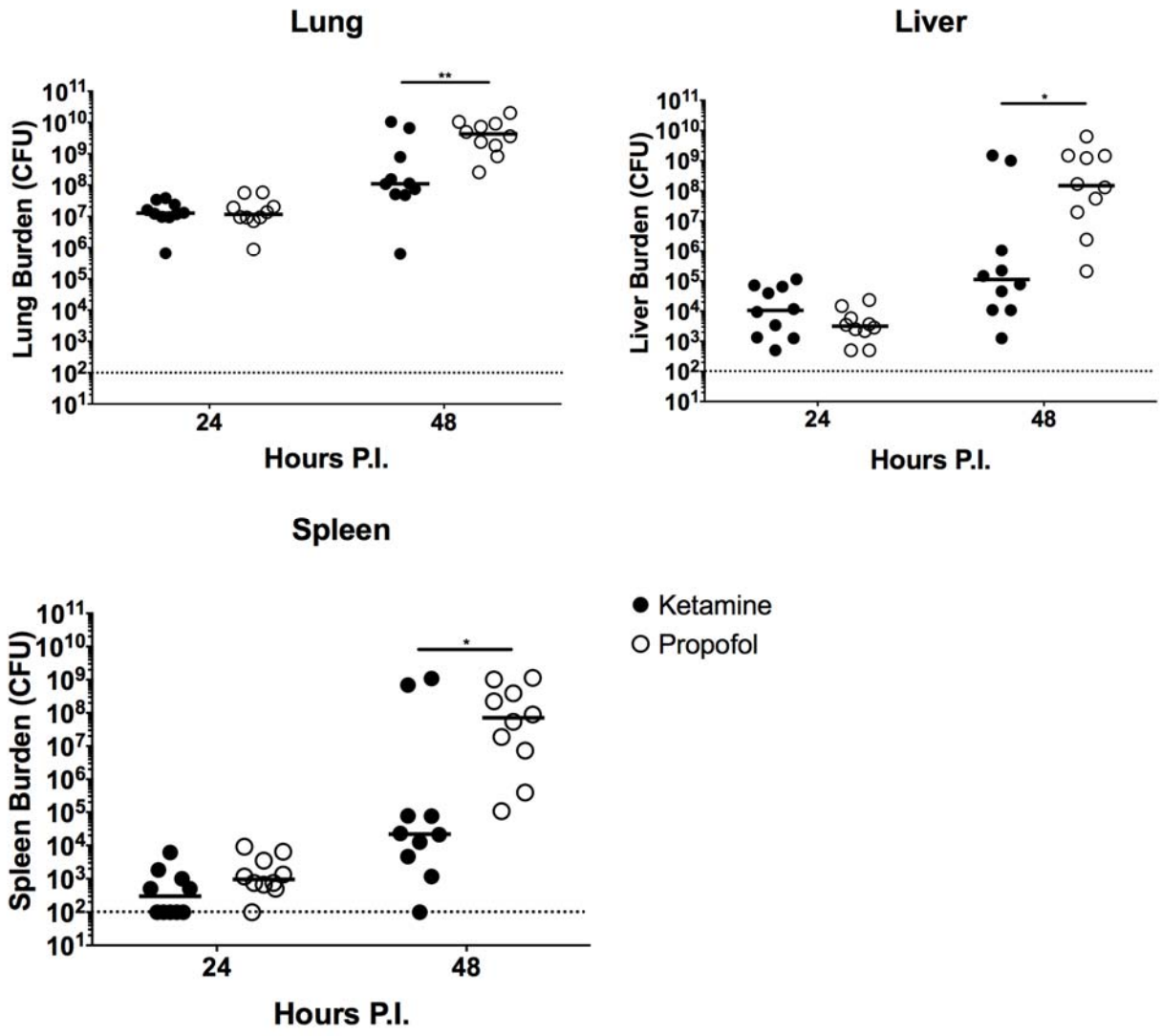
Lung
Lung Burden (CFU)
Hours P.I.
24
48
**
Liver
Liver Burden (CFU)
Hours P.I.
24
48
*
Spleen
Spleen Burden (CFU)
Hours P.I.
24
48
*
Ketamine
Propofol

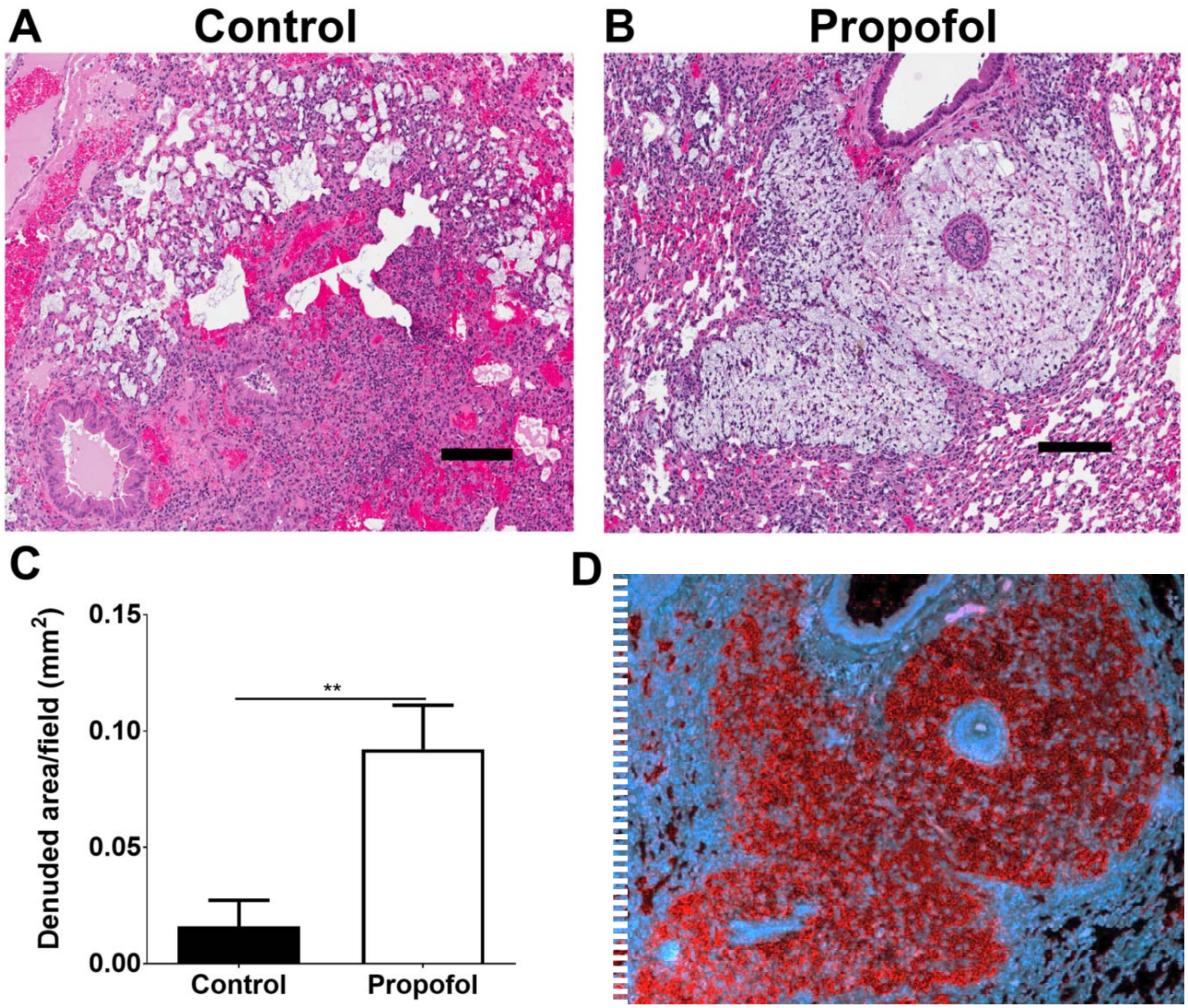
A
Control
B
Propofol
C
Denuded area/field (mm2)
0.15
0.10
0.05
0.00
**
Control
Propofol
D

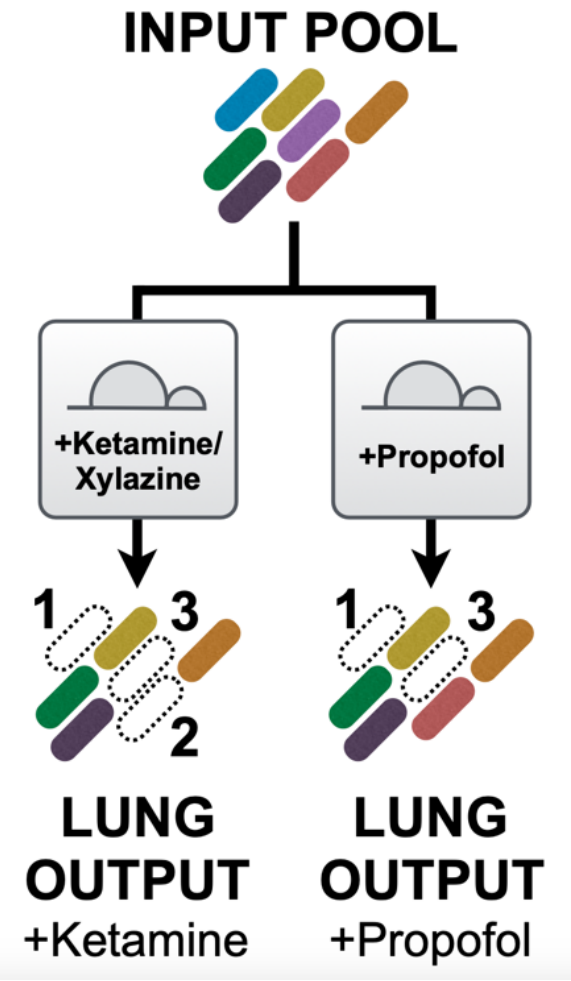
INPUT POOL
+Ketamine/
Xylazine
+Propofol
1
3
2
1
3
LUNG
OUTPUT
+Ketamine
LUNG
OUTPUT
+Propofol

B

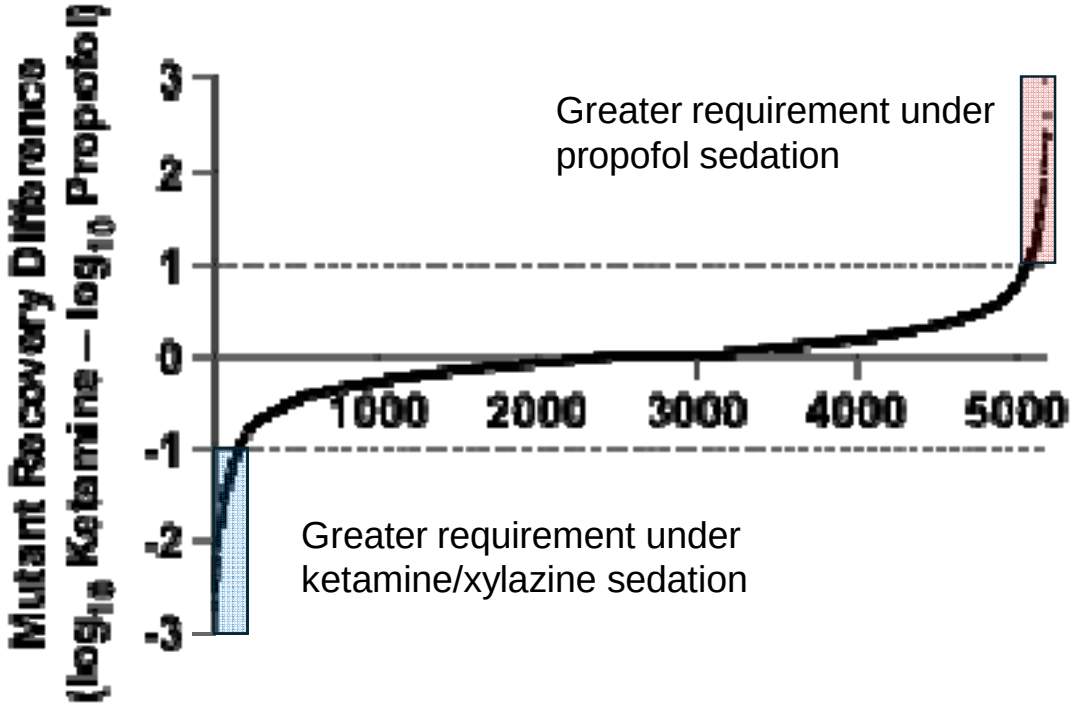
Mutant Recovery Difference
($\log_{10}$ Ketamine – $\log_{10}$ Propofol)
3
2
1
0
-1
-2
-3
1000
2000
3000
4000
5000
Greater requirement under
propofol sedation
Greater requirement under
ketamine/xylazine sedation

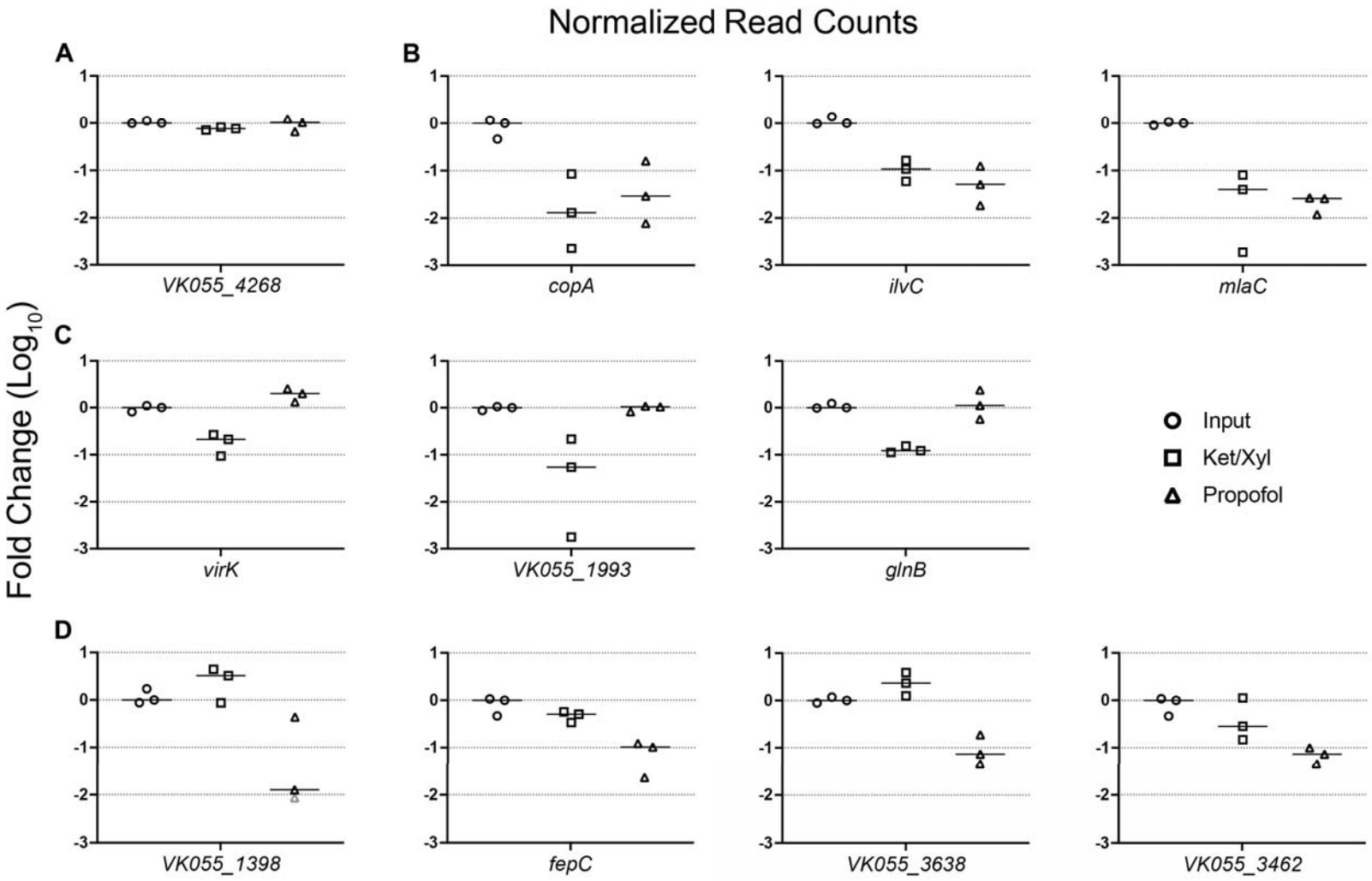
Normalized Read Counts
Fold Change (Log10)
A
B
C
D
VK055_4268
copA
ilvC
mlaC
virK
VK055_1993
glnB
VK055_1398
fepC
VK055_3638
VK055_3462
Input
Ket/Xyl
Propofol

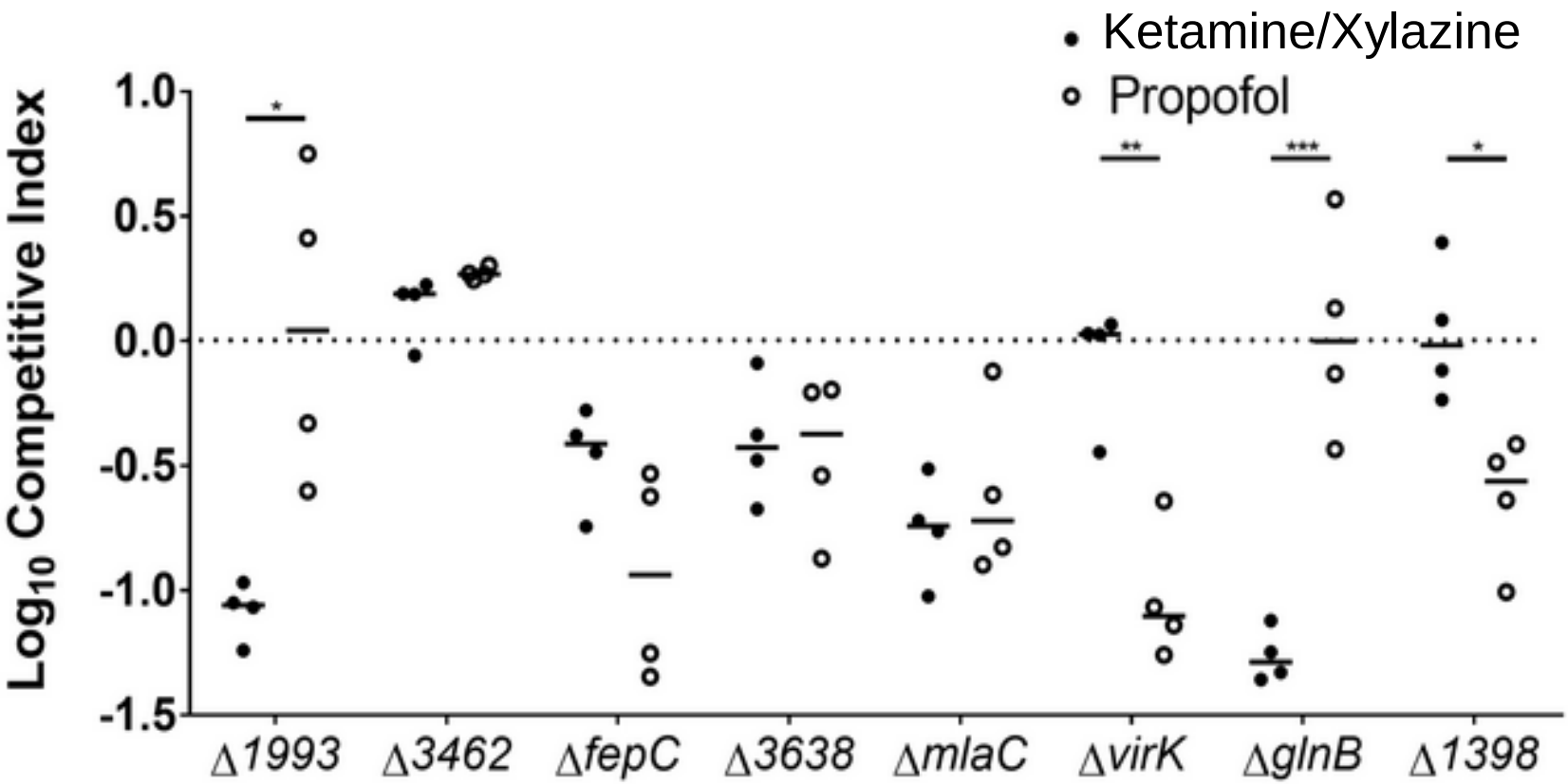
Ketamine/Xylazine
Propofol
Log10 Competitive Index
1.0
0.5
0.0
-0.5
-1.0
-1.5
*
**
***
*
Δ1993
Δ3462
ΔfepC
Δ3638
ΔmlaC
ΔvirK
ΔglnB
Δ1398

A

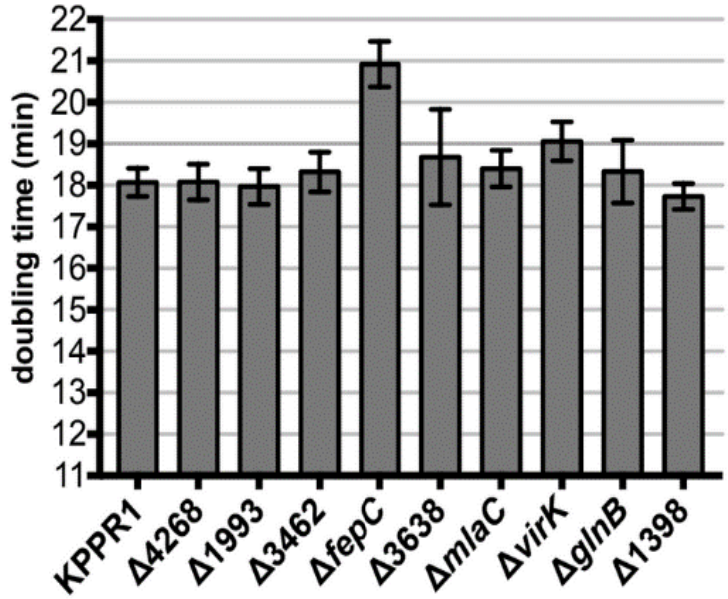
doubling time (min)
22
21
20
19
18
17
16
15
14
13
12
11
KPPR1
Δ4268
Δ1993
Δ3462
ΔfepC
Δ3638
ΔmlaC
ΔvirK
ΔglnB
Δ1398

B

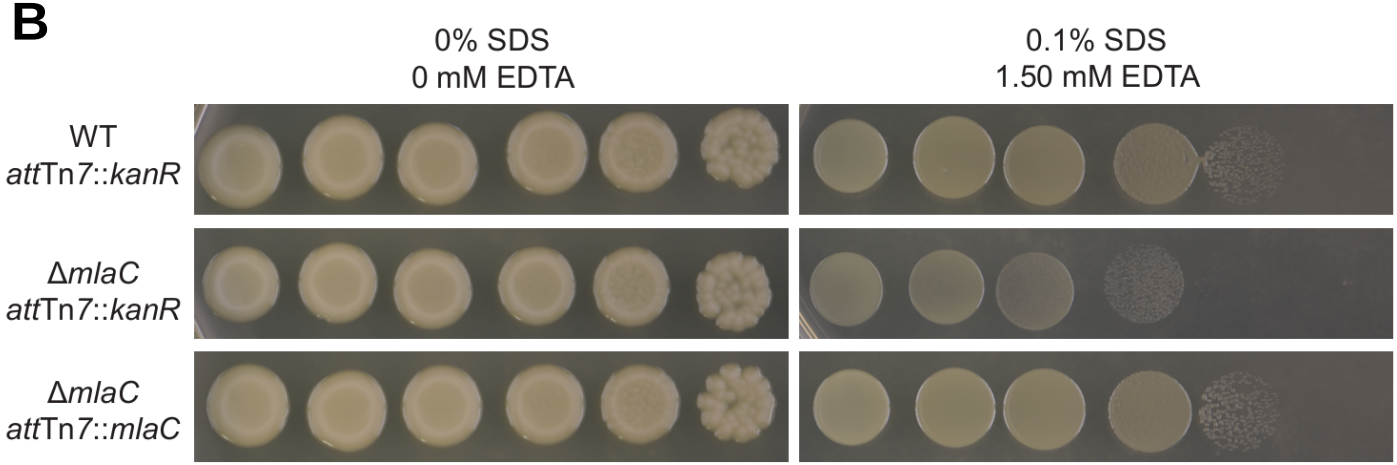
0% SDS
0 mM EDTA
0.1% SDS
1.50 mM EDTA
WT
attTn7::kanR
ΔmlaC
attTn7::kanR
ΔmlaC
attTn7::mlaC

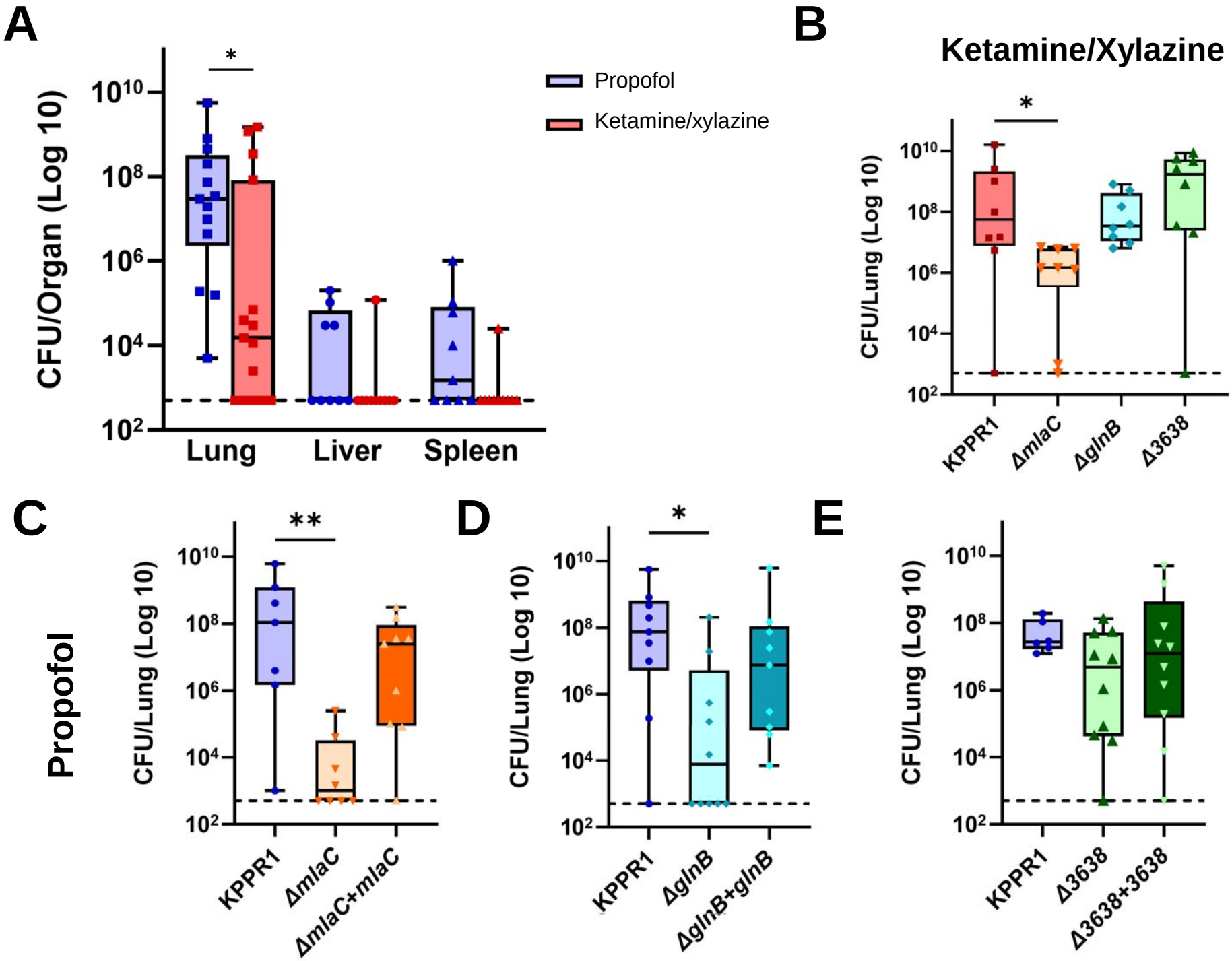
A
CFU/Organ (Log 10)
10^{10}
10^{8}
10^{6}
10^{4}
10^{2}
*
Lung
Liver
Spleen
Propofol
Ketamine/xylazine
B
Ketamine/Xylazine
CFU/Lung (Log 10)
*
KPPR1
ΔmlaC
ΔglnB
Δ3638
C
Propofol
CFU/Lung (Log 10)
**
KPPR1
ΔmlaC
ΔmlaC+mlaC
D
CFU/Lung (Log 10)
*
KPPR1
ΔglnB
ΔglnB+glnB
E
CFU/Lung (Log 10)
KPPR1
Δ3638
Δ3638+3638